Numerical Analysis of Shockwave Diffraction

Arnab Chaudhuri
Department of Aerospace Engineering & Engineering Mechanics, San Diego State University, 5500 Campanile Drive, San Diego, CA 92182, USA
Xiao Hong
School of Power and Energy, Northwestern Polytechnical University, X'ian, China
Gustaaf B. Jacobs
Department of Aerospace Engineering & Engineering Mechanics, San Diego State University, 5500 Campanile Drive, San Diego, CA 92182, USA

Arnab Chaudhuri: chaudhuri.arnab@gmail.com

Abstract This work reports analysis of complex shockwave diffraction and long-time behavior of shock-vortex dynamics over splitter geometry encountered in both external and internal compressible flows. The simulation resolved the experimental findings of literature and the insight of the flow topology is being presented with the probability density functions (PDFs) of various contributing terms of enstrophy transport equation and the invariants of the velocity gradient tensor. We use an artificial viscosity (AV) based explicit Discontinuous Spectral Element Method (DSEM) based compressible flow solver for this purpose. The numerical scheme utilizes entropy generation based artificial viscosity and thermal conductivity to simulate the conservative form of the governing compressible flow equations. A shock sensor based switch is used to reduce the addition of AV coefficients in rotation-dominated regions.

1 Introduction

Analysis of the mechanism of shockwave diffraction and shock-vortex interaction is of great interest to the shockwave community to utilize this knowledge in various engineering applications involving internal and external compressible flows. Numerical predictions with qualitative studies of shock diffraction over two-dimensional wedge and wall interaction of compressible vortex are reported in [1-5]. Nevertheless, studies related to the understanding of the mechanism of such complex dynamics are not abundant in literature. For example, Sun & Takayama [2] addressed the baroclinic and slip-stream vorticity generation in connection to the shock diffraction problems. On the other hand, Abate & Shyy [6] studied the dynamics of shock diffraction via numerical quantifications with the vorticity transport equation. They discussed the link between location of high strain rates and stress rates to solenoidal and dilatational dissipation rates of turbulent kinetic energies respectively. In these situations the baroclinic torque enhances the vorticity generation. It can be realized that, the viscous effects and small-scale turbulent dissipations are important for the long time evolution of primary vortex and subsequent smaller vortices generated from Kelvin-Helmholtz instability. The interactions of vortices with shocks and shock-lets also play important role in energy redistribution. Fomin [7] presented an interesting review of the evolution of the shock tube experimental facilities. Unsteady flow-separation behind a diffracting shock wave over curved walls and multi-faceted walls are presented in [8] and [9]. Experimental study of Quinn & Kontis [10] reported measurement of the static pressure for shock diffraction process. The detailed analysis of shock vortex dynamics related to the shock diffraction problems is still absent in the literature. The motivation of the present work is thus to shed

This is a post-peer-review, pre-copyedit version of a chapter published in ISSW 2017: 31st International Symposium on Shock Waves.
The final authenticated version is available online at: https://dx.doi.org/10.1007/978-3-319-91020-8_146

light on the complex dynamics of unsteady waves, coupled interactions like shock-shock, shock-vortex, vortex-vortex and shock-turbulence using high-fidelity numerical simulations. High order Weighted Essentially Non-Oscillatory (WENO), high-order discontinuous Galerkin methods (DGM) or DSEM are suitable numerical tools, on which one can rely upon. For example, unsteady studies exploiting WENO based solver can be found for application related to shockwave mitigation/propagation in [11, 12], shockwave focusing in [13] and nozzle flow separations in [14]. Noting the advantage of DGM and more general DSEM dealing with complex geometries with unstructured mesh arrangements, we employ DSEM to resolve the complex flow dynamics of the experimental observations reported in [15] and gain more insights of the flow mechanism. Since Gibb's phenomena are difficult handle in conjunction with DG and spectral methods, capturing shocks with DGM/DSEM in multi-dimensions subsequently gained much attention to the computational researchers. In their recent study, Chaudhuri et al. [16] presented the application of AV on shock capturing with DSEM for viscous shocked flows. In the present work, we use this entropy based AV method for a new detailed numerical study of shock diffraction over splitter geometry.

The paper is organized as follows. In section 2, a brief description of the governing equation and AV methodology recalled. The problem setup is given in the following section. Results and the transient flow analysis are presented in section 4. Finally, conclusions are drawn at the end in section 5.

2 Governing Equations and Numerical Method

The non-dimensional Navier-Stokes (NS) system of equations for compressible flow with artificial viscosity (AV) assumes the form given in Eq. (1). For the present study, we set viscosity and thermal diffusivity coefficients as zero. We thus solve the Euler system of equations with AV, estimated via entropy generation.

$$\frac{\partial U}{\partial t} + \nabla \cdot F^a(U) - \frac{1}{\mathrm{Re}_f} \nabla \cdot F^v(U) = 0 \qquad (1)$$

and

$$U = \begin{pmatrix} \rho \\ \rho\vec{V} \\ \rho E_t \end{pmatrix}, \qquad F^a(U) = \begin{pmatrix} \rho\vec{V} \\ \rho\vec{V}\vec{V} + p\overline{\overline{\delta}} \\ (\rho E_t + p\overline{\overline{\delta}})\vec{V} \end{pmatrix}, \qquad F^v(U) = \begin{pmatrix} 0 \\ \overline{\overline{\tau}} \\ \overline{\overline{\tau}}\vec{V} + \dfrac{\kappa_{eff}}{(\gamma-1)M_f^2 \mathrm{Pr}_f} \nabla T \end{pmatrix},$$

where, U is the conservative solution vector, F^a and F^v are the inviscid and viscous flux vectors respectively. ρ is the density, $\vec{V}$ is the velocity vector, E_t is the total internal energy, p is the static pressure and T is the temperature. γ is the ratio of specific heats, $\overline{\overline{\delta}}$ is the Kronecker delta tensor. M_f, Re_f and Pr_f are the reference Mach number, Reynolds number, and Prandtl number respectively. Assuming Stokes' hypothesis with zero bulk viscosity, the viscous shear stress tensor is expressed as $\overline{\overline{\tau}} = 2\mu_{eff} S - \frac{2}{3}\mu_{eff}(\nabla \cdot \vec{V})\overline{\overline{\delta}}$, where, $\mu_{eff} = \mu_h \mathrm{Re}_f + \mu$

is the effective dynamic viscosity and $S = \frac{1}{2}\left[\left(\nabla\vec{V}\right)^{\mathrm{T}} + (\nabla\vec{V})\right]$ is the symmetric part of velocity gradient tensor (here the superscript 'T' designates a transpose). Similarly, the effective thermal conductivity is given by $\kappa_{eff} = \kappa_h \mathrm{Re}_f + \kappa$. Finally, the ideal gas equation of state, $P = \rho T / (\gamma M_f^2)$, closes Eq. (1). In this study, we set $\gamma = 1.4$, $M_f = 1$ and $\mathrm{Pr}_f = 0.72$.

The overall idea of an AV method is to add a high order dissipation term to stabilize the numerical scheme in the vicinity of shocks. We scale AV coefficients with viscous and thermal entropy generation terms of the viscous entropy transport equation (see detail in [16]). We also limit the artificial coefficients by setting the upper bounds to ensure that the inviscid time step remains smaller than the viscous time step. The staggered multidomain DSEM, in nodal collocation formulation involves finding solution vector on the Chebyshev-Gauss quadrature points while fluxes are computed on the Chebyshev-Lobatto quadrature points of the mapped computational elements.

3 Problem setup

We consider a non-dimensional rectangular domain of 6.6×2.227 in two-dimensional (2D) x-y plane with a splitter plate of thickness ≈ 1.956 and wedge angle 8°. These are similar to those reported for experimental setup in [15]. A shock wave with a Mach number $M_s = 1.59$ is allowed to pass through the lower-half section of the splitter plate. The initial conditions are prescribed using Rankine-Hugoniot relation for stagnant state (1) and shocked gas state (2) with the initial shock location at $x_s = 1.8$. The left and right boundaries are situated sufficiently far to avoid any reflection on the zone of analysis and the initial states and are fixed at those boundaries. We set symmetry conditions for the rest of the boundaries. Time snaps are saved to match the corresponding data with the experimental results. The reference state ϕ_f, is taken as the stagnant state conditions at state (1), ϕ_1, to satisfy $M_f = 1$ and reference length is taken as the height of the shock-tube of the experiment $L_f = 24.8$ mm. We have taken 57,350 P3 (fourth order) elements with total 0.9176×10^6 number of degrees of freedom within the domain. The elements are having a size of $\approx 0.01^2$ in the main interaction zone and are stretched outwards. The zone of the analysis thus contains a mesh resolution of 20 μm to 130 μm. In this work, the value of the CFL number is taken as 0.9 and the model constants for AV are set as: $\left(C_\mu, C_\kappa, C_m\right) = \left(0.5,\ 0.25,\ 0.15\right)$. The details about the model constants of AV can be found in [16].

4 Results and Discussion

We first compare the experimental Schlieren of [15] with the numerical Schlieren of the present simulation (see Fig. 1a). An excellent agreement can be seen between the two at time instant $t_4 = 3.098$. The initial time evolution (not shown) is also found to be in very good agreement with the experimental results. The present simulation captures the essential features of the shock dynamics and the shock-vortex interaction. Fig. 1b shows the basic flow visualization in terms of rotation-dominated region of the flow-field. Here we plotted the

contours of strain-enstrophy angle $\psi = \tan^{-1}\left(\frac{S \cdot S}{A \cdot A}\right)$. A is the anti-symmetric part of the velocity gradient tensor. Note that, the blue colored regions are associated with lower values of ψ. This clearly indicates the rotation dominated vortex core regions of the flow-field. In the next section we present the flow-analysis from the data window as shown in Fig. 1b.

The enstrophy (Ω) transport equation for viscous compressible flows with constant transport properties along with the AV coefficients (non-dimensional form) is given by,

$$\frac{\partial \Omega}{\partial t} = -\nabla \cdot \left(\vec{V}\Omega\right) + \vec{\omega} \cdot S \cdot \vec{\omega} - \Omega\left(\nabla \cdot \vec{V}\right) + \vec{\omega} \cdot \left[\frac{\nabla\rho \times \nabla p}{\rho^2}\right] - \vec{\omega} \cdot \left[\frac{\mu_h \,\mathrm{Re}_f + \mu}{\mathrm{Re}_f}\left\{\frac{4}{3}\frac{1}{\rho^2}\nabla\rho \times \left[\nabla\left(\nabla \cdot \vec{V}\right)\right] - \frac{1}{\rho^2}\nabla\rho \times \left(\nabla \times \vec{\omega}\right) - \frac{1}{\rho^2}\nabla^2\vec{\omega}\right\}\right] \tag{2}$$

where, $\vec{\omega}$ is the vorticity vector.

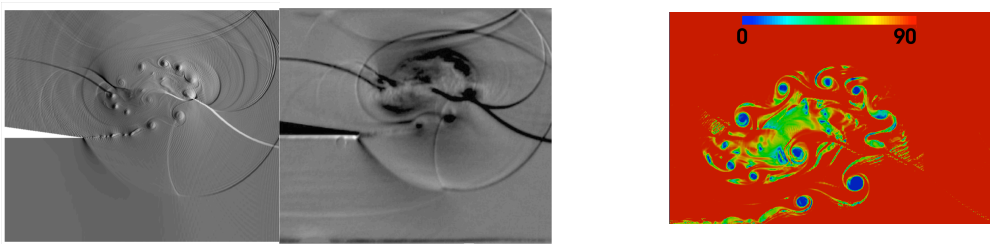

(a) (b)

Fig. 1 (a) Comparison of numerical (left) and experimental [18] schlieren (right) pictures, (b) Contours of strain-enstrophy angle (window for analysis).

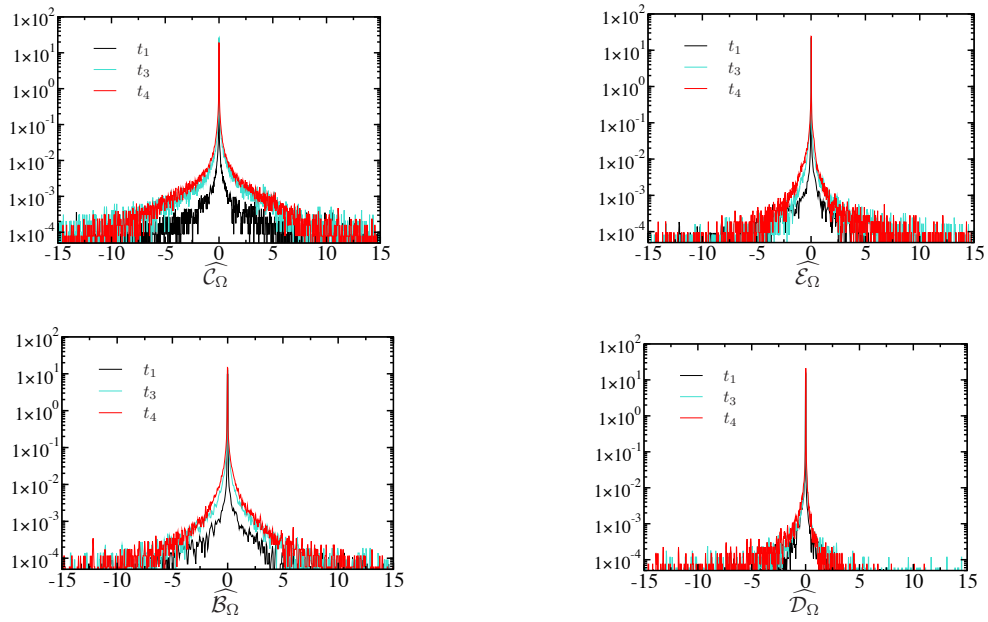

Fig. 2 PDFs (all vertical axes) of various terms: budget terms of enstrophy transport equation, ($t_1 = 0.578$, $t_3 = 2.258$, $t_4 = 3.098$).

The first three terms of the right hand side of Eq. (2) can be expressed in term of Lamb vector $L = \vec{\omega} \times \vec{V}$ as $\vec{\omega} \cdot \nabla \times L = \nabla \cdot \left(\vec{V} \Omega \right) - \vec{\omega} \cdot S \cdot \vec{\omega} + \Omega \left(\nabla \cdot \vec{V} \right)$. The second term of the right hand side of the Eq. (2) is known as the vortex stretching term and is zero in 2D flow-field. In the following figures, we compare the other terms, namely, the enstrophy convection: C_Ω (first term), the vortex expansion: E_Ω (3rd term), the Baroclinic term: B_Ω (4th term) and the diffusion term: D_Ω (5th term). With the present AV methodology, the contribution of the diffusion term is active with non-zero μ_h. The PDFs of the standardized variables of these quantities are illustrated in Fig. (2) at different time instant. It can be seen that all PDF's exhibit very high intermittent character with high flatness values. The skewness of $\hat{D}_\Omega$ is negative throughout. The distribution of $\hat{C}_\Omega$ is near symmetric with low negative skewness values. During the initial growth regime of the enstrophy, E_Ω and B_Ω override the other terms with positive skewness values. The divergence of the Lamb vector can be expressed as: $\nabla \cdot L = \vec{V} \cdot \nabla \times \vec{\omega} - \vec{\omega} \cdot \vec{\omega}$. It is evident that positive flexion product, $F = \vec{V} \cdot \nabla \times \vec{\omega}$, is associated with positive $\nabla \cdot L$. We also observed highly peaked PDF of divergence of the Lamb vector (not shown) with positive skewness, which evolves towards the near symmetric shape at the later stage. The joint PDF of divergence of the Lamb vector and the enstrophy is shown in Fig. 3. The asymmetric distribution with negative correlation coefficients clearly depicts the association of vortex core regions with the negative $\nabla \cdot L$.

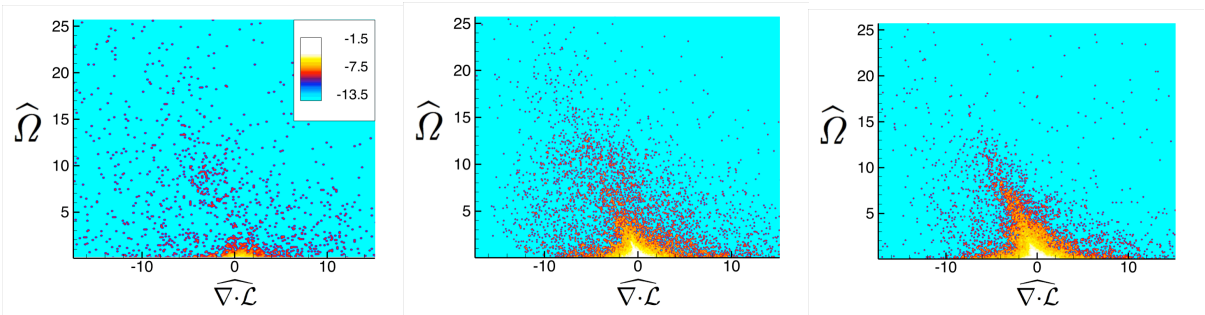

Fig. 3 Joint PDFs of divergence of Lamb vector with enstrophy at t_1, t_3, t_4. Contour levels are in log of joint PDF.

5 Conclusions

In this work, we made an initial attempt to resolve complex shock-vortex interaction via high-fidelity numerical simulation and made a novel analysis for understanding the mechanism of the flow-evolution related to shock diffraction over splitter geometry. An excellent agreement between the numerical findings and the experimental results of literature is found. The Euler system of equation is solved with high-order DSEM solver equipped with entropy generation based AV coefficients. We analyzed the non-dimensional enstrophy transport equation for the viscous compressible flows. The diffusive term of this equation is active based on AV of the present scheme. All component terms of the transport equation are compared via the PDFs.

The PDF of divergence of Lamb vector shows an overall positive skewness and its anti-correlation with enstrophy reveals the association of negative values of divergence of the Lamb vector with vorticity cores. Extension of this work will be carried for further understanding of the evolution of the flow topology of the complex dynamics. Subsequent 3D study will be the next phase of our work for understanding and quantifying the role of AV in resolving complex multi-dimensional interactions like transverse-waves, shocklet-vortex, shock-turbulent fluctuation and small-scale viscous dissipations.

Acknowledgement

This work used the resource of Extreme Science and Engineering Discovery Environment (XSEDE) [17] supported by the National Science Foundation of USA, Grant number ACI-1053575. The authors greatly acknowledge the collaboration with W. S. Don of Ocean University of China and F. Mashayek of University of Chicago.

References

[1] M. Sun, K. Takayama, Shock Waves **13**(1), 25 (2003)
[2] M. Sun, K. Takayama, Journal of Fluid Mechanics **478**, 237 (2003)
[3] P. Halder, S. De, K. Sinhamahapatra, N. Singh, Shock Waves **23**(5), 495 (2013)
[4] T. Murugan, S. De, A. Sreevatsa, S. Dutta, Shock Waves **26**, 311 (2016)
[5] R. Ripley, F.S. Lien, M. Yovanovich, Computers & fluids **35**(10), 1420 (2006)
[6] G. Abate, W. Shyy, Progress in Aerospace Sciences **38**(1), 23 (2002)
[7] N. Fomin, Journal of Engineering Physics and Thermophysics **83**(6), 1118 (2010)
[8] C. Law, A. Muritala, B. Skews, Shock Waves **24**(3), 283 (2014)
[9] B.W. Skews, Shock waves **14**(3), 137 (2005)
[10] M.K. Quinn, K. Kontis, Sensors **13**(4), 4404 (2013)
[11] A. Chaudhuri, A. Hadjadj, O. Sadot, G. Ben-Dor, Shock Waves **23**(1), 91 (2013)
[12] A. Chaudhuri, A. Hadjadj, O. Sadot, E. Glazer, International Journal for Numerical Methods in Engineering **89**(8), 975 (2012)
[13] M. Shadloo, A. Hadjadj, A. Chaudhuri, Physics of Fluids **26**(7), 076101 (2014)
[14] A. Chaudhuri, A. Hadjadj, Aerospace Science and Technology **53**, 10 (2016)
[15] F. Gnani, K. Lo, H. Zare-Behtash, K. Kontis, Acta Astronautica **99**, 143 (2014)
[16] A. Chaudhuri, G. Jacobs, W. Don, H. Abbassi, F. Mashayek, Journal of Computational Physics **332**, 99 (2017).
[17] J. Towns, T. Cockerill, M. Dahan, I. Foster, K. Gaither, A. Grimshaw, V. Hazlewood, S. Lathrop, D. Lifka, G.D. Peterson, et al., Computing in Science & Engineering **16**(5), 62 (2014)